frontiers in Materials

ORIGINAL RESEARCH
published: 16 February 2016
doi: 10.3389/fmats.2016.00009

Carbon Materials as Additives to WO_3 for an Enhanced Conversion of Simulated Solar Light

*Rocio J. Carmona[1], Leticia F. Velasco[2], Enzo Laurenti[3], Valter Maurino[3] and Conchi O. Ania[1]**

[1] ADPOR Group, Instituto Nacional del Carbón (INCAR-CSIC), Oviedo, Spain, [2] Department of Chemistry, Royal Military Academy, Brussels, Belgium, [3] Department of Chemistry, Università di Torino, Turin, Italy

We have explored the impact of the incorporation of nanoporous carbons as additives to tungsten oxide on the photocatalytic degradation of two recalcitrant pollutants: rhodamine B (RhB) and phenol, under simulated solar light. For this purpose, WO_3/carbon mixtures were prepared using three carbon materials with different properties (in terms of porosity, structural order and surface chemistry). Despite the low carbon content used (2 wt.%), a significant increase in the photocatalytic performance of the semiconductor was observed for all the catalysts. Moreover, the influence of the carbon additive on the performance of the photocatalysts was found to be very different for the two pollutants. Carbon additives of hydrophobic nature increased the photodegradation yield of phenol compared to bare WO_3, likely due to the higher affinity and stronger interactions of phenol molecules toward basic nanoporous carbons. Oppositely, the use of acidic carbon additives led to higher RhB conversions due to increased acidity of the WO_3/carbon mixtures and the stronger affinity of the pollutant for acidic catalyst's surfaces. As a result, the photooxidation of RhB is favored by means of a coupled (photosensitized and photocatalytic) degradation mechanism. All these results highlight the importance of favoring the interactions of the pollutant with the catalyst's surface through a detailed design of the features of the photocatalyst.

Keywords: tungsten oxide, nanoporous carbons, heterogeneous photocatalysis, photosensitization, simulated solar light

OPEN ACCESS

Edited by:
Ángel Berenguer-Murcia, Universidad de Alicante, Spain

Reviewed by:
Benjaram M. Reddy, CSIR – Indian Institute of Chemical Technology, India
Sotiris Sotiropoulos, Aristotle University of Thessaloniki, Greece
Antonio Monari, Université de Lorraine, France

****Correspondence:***
Conchi O. Ania
conchi.ania@incar.csic.es

Specialty section:
This article was submitted to Carbon-Based Materials, a section of the journal Frontiers in Materials

Received: *14 December 2015*
Accepted: *01 February 2016*
Published: *16 February 2016*

Citation:
Carmona RJ, Velasco LF, Laurenti E, Maurino V and Ania CO (2016) Carbon Materials as Additives to WO_3 for an Enhanced Conversion of Simulated Solar Light. Front. Mater. 3:9. doi: 10.3389/fmats.2016.00009

INTRODUCTION

WO_3 is a *n*-type semiconductor usually presenting a three-dimensional arrangement of slightly distorted corner-shared [WO_6] octahedra derived from ideal cubic perovskite (type ReO_3), which is responsible of its electrooptical, electrochromic, ferroelectric, and catalytic properties (Svensson and Granqvist, 1984; Cotton and Wilkinson, 1988; Kumar and Rao, 2015).

It is considered an interesting material as a stable visible light driven photocatalyst for an efficient degradation of recalcitrant organic compounds due to its relatively large abundance, non-toxicity, physical and chemical resilience in harsh environments, and most importantly its strong absorption within the solar spectrum (i.e., band gap between 2.4 and 2.8 eV), and high oxidation power of the photogenerated holes (+3.1 −3.2 vs. NHE) due to a deep valence band. Nevertheless, pure WO_3 has lower light energy conversion efficiency – compared to titania – as the reduction potential of

the photogenerated electrons in the conduction band of WO_3 is relatively low, being inadequate for O_2 reduction. This inherent characteristic provokes the accumulation of the electrons on the surface of the material, and therefore an increase in the recombination rate of these photogenerated electrons with holes, ultimately reducing its photocatalytic and performance (Irie et al., 2008; Nosaka et al., 2011; Wen et al., 2013).

Several strategies have been adopted to compensate for this limitation of WO_3 as photocatalyst, including surface and interface modification, particle size and morphology control, composite and hybrid materials, transition/noble metal doping, surface sensitization (Ho et al., 2012; Wicaksana et al., 2014; Spurgeon et al., 2014), and the use of photoelectrochemical approaches based on the application of a bias potential or association with a photocathode – i.e., with a p-type semiconductor electrode – or a photovoltaic cell suited for the realization of a water splitting system under solar illumination (Gratzel, 2001; Bignozzi et al., 2013). All these approaches aim to increase the electron trapping, to inhibit the charge recombination, and to increase the selectivity of a particular product so as to improve the efficiency of photocatalytic processes. In this study, we have investigated the incorporation of carbon materials as additives to WO_3 as an alternative to improve its photocatalytic performance. Based on the high electronic density of carbon materials, provided by the stacked graphene-layers, it seems reasonable to anticipate that the accumulation of electrons can be dissipated by delocalization in the π-electron density of the graphitic structure of carbons. Indeed, the use of carbons as additives to semiconductors has been widely explored (Faria and Wang, 2009; Leary and Westwood, 2011; Ania et al., 2012; Velasco et al., 2014) mostly to TiO_2 and ZnO, and several studies report the enhanced photoconversion yield of the semiconductor/carbon catalysts. In most cases, the improved performance is attributed to mass transfer effects (especially when using porous additives) and/or interfacial electronic effects in the case of highly conductive carbon materials such as graphenes and carbon nanotubes (Faria and Wang, 2009; Leary and Westwood, 2011; Ania et al., 2012; Velasco et al., 2014). More recently, we have demonstrated the photochemical activity of certain nanoporous carbons due to their ability to promote the photochemical splitting of water (Ania et al., 2014; Velasco et al., 2014) and generate oxygen radical species capable of reacting with electron donors (i.e., pollutant in aqueous solution), hence boosting the photooxidation conversion (Velasco et al., 2012; Velasco et al., 2013a).

Considering all the above, the objective of this work was to investigate the use of several carbon additives of varied characteristics in the performance of WO_3/carbon photocatalysts under simulated solar light. The catalysts were prepared by adding ca. 2 wt.% of various carbon materials to WO_3 powders; the carbon additives were chosen based of their different structural order and graphitic structure, ranging from nanoporous carbons with an ill-defined graphitic structure to conductive carbon nanotubes. The novelty of the work is to provide a deep insight on the role of carbon additives of varied nature on the photocatalytic performance of the hybrid WO_3/carbon photocatalysts for the degradation of two recalcitrant pollutants showing a low photoconversion under visible light (i.e., phenol) and a cationic dye [i.e., rhodamine B (RhB)]. Our results provide new insights on the different behavior of the carbon additives for each pollutant, pointing out the importance of the adequate choice of the carbon additive depending on the nature of the pollutant and the interactions at the catalyst–pollutant interface, which are strongly controlled by the characteristics of all the photocatalyst components.

MATERIALS AND METHODS

Materials

Commercially available WO_3 powders (Sigma Aldrich) were used in the preparation of the WO_3/carbon photocatalysts. The carbon additives were selected upon their differences in porosity, composition, and structural order: a nanoporous carbon prepared by chemical activation of a lignocellulosic residue (sample CL), a hydrochar obtained from hydrothermal carbonization of sucrose at 180°C (sample HC) (Velasco et al., 2013b) and multiwall carbon nanotubes (sample CNT, Nanocyl, average nanotubes diameter 9.5 nm, average length 1.5 mm). Further characterization of the carbon additives (morphology, porosity, structure) is compiled in **Table 1** and (Figures S1 and S2 in Supplementary Material). WO_3/carbon catalysts with 2 wt.% of carbon additive were prepared by physical mixture of the semiconductor powders with the as-received carbons in a mortar. The distribution of the carbon additives within the semiconductor matrix was confirmed by SEM-EDX images (**Figure 1**). The catalysts are labeled as WO_3/X, where X stands for the carbon material.

Characterization Techniques

The porosity of the samples was measured by N_2 adsorption isotherms at −196°C (Figure S1 in Supplementary Material); the samples were previously outgassed under vacuum (ca. 10^{-3} Torr) at 120°C overnight. The isotherms were used to calculate the specific surface area (S_{BET}) and pore volumes (V_{total} and micropore volume, W_o, using the Dubinin–Radushkevich equation) (Rouquerol et al., 2014).

The surface chemistry was characterized by the determination of the pH at the point of zero charge (pH_{PZC}) (Ania et al., 2007) and the hydrophobic character; the latter was determined

TABLE 1 | Main textural parameters obtained from gas adsorption data and surface chemistry parameters of the studied materials (semiconductors, carbon materials, and semiconductor/carbon catalysts).

	S_{BET} (m^2 g^{-1})	V_{PORES}[a] (cm^3 g^{-1})	Wo[b] (cm^3 g^{-1})	pH_{pzc}	HI
WO_3	6	0.038	0.002	4.3	0.2
WO_3/HC	12	0.056	0.003	4.2	0.7
WO_3/CL	32	0.072	0.011	4.0	0.7
WO_3/CNT	18	0.094	0.006	4.7	2.4
HC	8	0.014	0.001	4.3	1.2
CL	1280	1.030	0.270	3.6	1.4
CNT	298	2.090	0.200	8.6	7.7

[a]*Total pore volume evaluated from the N_2 adsorption isotherms at 77 K at a relative pressure of 0.99.*

[b]*Micropore volume evaluated from the Dubinin–Radushkevich method applied to the N_2 adsorption isotherms.*

See further characterization details in Figures S1–S3 in Supplementary Material.

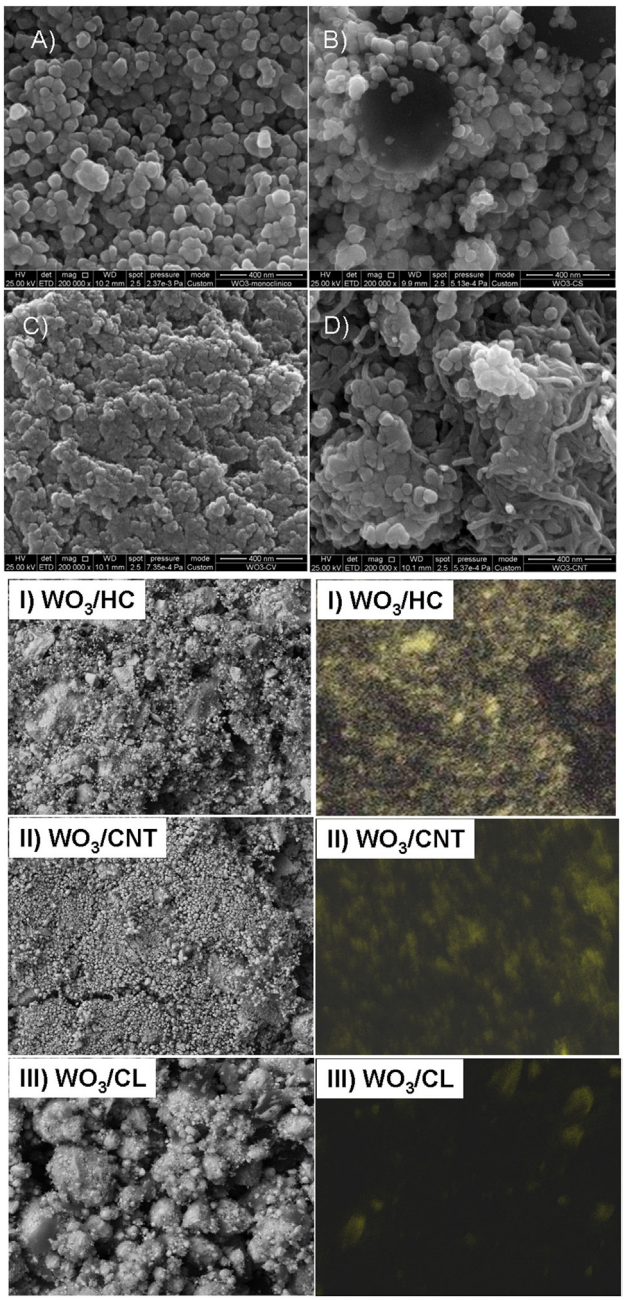

FIGURE 1 | SEM images (A–D) and EDX mapping (I, II, III) showing the distribution of the carbon additives on the photocatalysts: (A) WO_3, (B) WO_3/HC, (C) WO_3/CL, (D) WO_3/CNT.

by comparing their affinity to adsorb water and benzene and defining the surface hydrophobicity index (HI) as the ratio of the amount of benzene adsorbed to that of water. Predetermined amounts of dry samples were exposed to either water or benzene vapors in air-tight environments for 24 h at ambient temperature. The amounts adsorbed after 24 h were measured gravimetrically using a Setaram instrument thermal analyzer, recording the weight loss in nitrogen between 30 and 400°C. The optical features of the catalysts were determined by UV-Vis diffuse reflectance spectroscopy, recorded on a Shimadzu spectrometer equipped with an integrating sphere and using $BaSO_4$ as a blank reference. Measurements were recorded in the diffuse reflectance mode (R) and transformed to a magnitude proportional to the extinction coefficient through the Kubelka–Munk function, $F(R\infty)$ (Kubelka, 1948). Band-gap energies were calculated by plotting $[F(R\infty)\cdot h\upsilon]^{1/n}$ against $h\upsilon$ (best fitting was obtained for $n = 1/2$ characteristic of direct allowed transitions). Raman spectroscopy was performed on a high resolution Jobin Yvon Horiba Raman spectrometer equipped with a Leica microscope by excitation with green laser light (532 nm) in the range between 1000 and 3500 cm^{-1} using typical exposure times of 5 s (Figure S2 in Supplementary Material). The morphology of the samples was observed by Field Emission Gun Scanning Electron Microscopy (FEG-SEM) with an X-ray Energy-Dispersive System (EDS) in a JEOL JSM-7001F, and in a FE-SEM apparatus (QuantaSEM, FEI), using an accelerating voltage of 25 kV.

Photodegradation Runs

The photocatalytic activity of the samples was evaluated toward the degradation of RhB (5 ppm) and phenol (50 ppm) in water using a batch reactor (250 mL) illuminated by a UV-Vis lamp [300 W, Osram Ultra-Vitalux, incident photon flux measured by chemical actinometry (Kuhn et al., 2004) was 3.7×10^{-6} einsteins/s] with a sunlike radiation spectrum, vertically suspended above the reactor. All prepared catalysts were gently homogenized in a mortar before being dispersed in the solution. Before each experiment, suspensions of the catalysts (ca. loadings of 0.5 and 1 g/L) were initially equilibrated under mechanical stirring (900 rpm) and darkness in solution to allow adsorption of the pollutant in the porosity of the materials, and then irradiated for 120 min providing a constant air flow of ca. 50 mL/min to ensure a constant oxygen concentration in the solution. All the experiments were done in duplicate with deviations below 5% in all cases; reported data represent the average values. Furthermore, the initial concentration was adjusted considering the uptake of each catalyst so as to achieve the same initial concentration of the pollutant in solution at the beginning of the illumination period. This procedure allows to isolate the yield of the photooxidation reaction from the effects of concentration on adsorption and direct photolysis.

During the irradiation, small aliquots of the solution (~1 cm^3) were taken out at predetermined time intervals and analyzed by spectrophotometry and reverse-phase HPLC [Spherisorb C18 column 125 mm × 4 mm, methanol to water (H_3PO_4 0.1 M) 5:95, 30°C, 0.7 cm^3/min flow rate, photodiode array detector using the corresponding wavelengths] to determine the residual concentration of phenol (269 nm) and its aromatic degradation products, namely quinones (1,4-benzoquinone, 245 nm and 1,4 dihydroxybenzene, 288 nm), 1,2-dihydroxybenzene (*o*-catechol, 275 nm), 1,3-dihydroxybenzene (resorcinol, 273 nm), 1,3,5-trihydroxybenzene (264 nm), and 1,2,4-trihydroxybenzene (482 nm) (all Aldrich 99% reagents). The samples were previously filtered using cellulose filters having mean pore size of 0.45 μm. All the experiments were done in duplicate with deviations below 5% in all cases; reported data represent the average values. Blank assays in the absence of catalysts (direct photolysis) were also carried out

for both pollutants for comparison purposes. Furthermore, the stability of the catalysts under illumination was also evaluated, with no evidences of changes in the composition or the structure of the carbon component detected by XPS and XRD analysis.

RESULTS AND DISCUSSION

We have explored the role of carbon additives of varied properties on the performance and stability of WO_3/carbon catalysts for the photooxidation of two recalcitrant pollutants of different characteristics, phenol and RhB, in solution using simulated solar light. A more elaborated discussion on the physicochemical properties of the nanoporous carbons used as additives has been reported in a previous study (Carmona et al., 2015) (see also Supplementary Material); however, selected properties are herein shown for data interpretation purposes. Briefly, the high resolution SEM images and EDX analysis of the WO_3/carbon catalysts evidence the homogeneous distribution of the carbon additive within the semiconductor matrix (**Figure 1**), showing the good contact between both phases (carbon and inorganic particles) despite the low amount of additive and the synthetic procedure by physical mixture. Furthermore, the incorporation of carbon additives did not modify the optical features of the semiconductor, as detected by UV-Vis diffuse reflectance spectroscopy (**Figure 2**), which is expected as the WO_3/carbon catalysts were prepared by physical mixture of both components. Indeed, the spectrum of WO_3 presented the characteristic absorption sharp edge at 470 nm that corresponds to a band-gap of 2.6 eV, in agreement with the values reported in the literature (Kopp et al., 1977; Bullett, 1983; Svensson and Granqvist, 1984; Cotton and Wilkinson, 1988; Hjelm et al., 1996; Irie et al., 2008; Nosaka et al., 2011; Kumar and Rao, 2015). The spectra corresponding to the WO_3/carbon catalysts showed similar profiles below 500 nm, with the sharp edge around 470 nm characteristic of the bare semiconductor. Only in the case of WO_3/CNT, a slight shift of ca. 20 nm in the absorption sharp edge was detected as the samples are prepared by physical mixture; it is unlikely (but may not be discarded) to have an optimized interface between both phases of this catalyst that would favor the absorption of low energy photons.

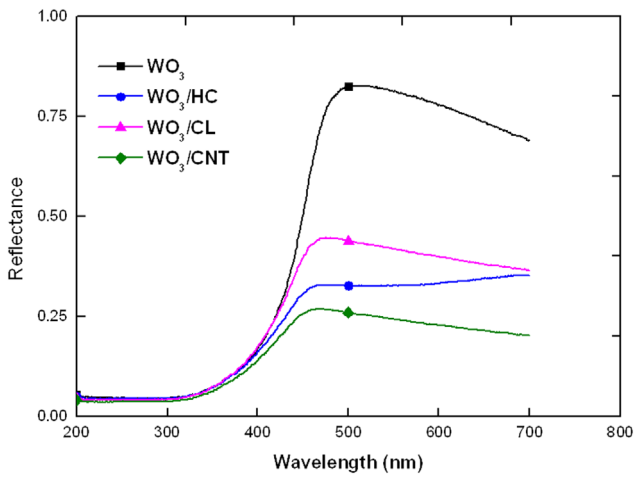

FIGURE 2 | Diffuse reflectance spectra of the studied photocatalysts.

However, the profiles of the WO_3/carbon catalysts showed a marked increase in the absorbance in the region between 500 and 800 nm, regardless the nature of the carbon, a characteristic feature associated with the strong light absorption of black opaque materials (Araña et al., 2003; Carmona et al., 2015). The trend for the absorption above 500 nm followed the order: CNT > HC > CL.

The performance of the studied catalysts was compared to that of direct photolysis of the pollutants in solution. In both cases, the photooxidation in the absence of catalyst was poorly efficient (**Table 2**) as inferred from their corresponding conversion values (ca. 1.7 and 21% for phenol and RhB, respectively). The photolytic breakdown was larger in the case of RhB, as expected based on the optical features of the pollutants (see Figure S3 in Supplementary Material) and due to the characteristics of the irradiation source (Figure S4 in Supplementary Material), as it will be discussed below.

Phenol Photodegradation

Figure 3 shows the evolution of phenol concentration upon irradiation of aqueous suspensions of WO_3 and WO_3/carbon mixtures with catalyst loadings of 0.5 and 1 g/L. As seen, the incorporation of WO_3 increased the photoconversion of phenol compared to direct degradation from solution in the absence of catalyst, although the value was quite low (below 2%). This is somewhat reasonable considering that the low absorption features of phenol in the visible light region (Figure S3 in Supplementary Material), and the fact that the irradiation lamp used emits mostly above 400 nm (only ca. 8% of the incident flux of the lamp corresponds to the UV range, Figure S4 in Supplementary Material). The incorporation of carbon additives improved the photooxidation yield, particularly in the case of the carbon nanotubes. Although phenol conversion values are still quite low (**Figure 3**), which is due to the fact that phenol is a recalcitrant compound that is not easily degraded under visible light, there is a marked increase in conversion upon the incorporation of the catalysts (from 2 to 10%). This is most outstanding as it shows the beneficial effect of the catalyst, and more specifically that of the carbon additives used.

Increasing the catalyst loading from 0.5 to 1 g/L did not enhance the performance of any of the studied photocatalysts, with the

TABLE 2 | Conversion values (%) of phenol and Rhodamine B achieved after 2 h of irradiation of the studied photocatalysts at two catalyst loadings (ca. 0.5 and 1 g/L).

	Conversion values (%)			
	Phenol		Rhodamine B	
Direct photolysis	1.7		21.4	
Catalyst loading (g/L)	**0.5**	**1**	**0.5**	**1**
WO_3	2.4	3.0	37.6	36.9
WO_3/HC	3.2	2.5	51.8	43.4
WO_3/CL	4.5	3.4	72.8	54.7
WO_3/CNT	7.0	7.4	47.4	55.4

Data corresponding to the direct photolytic degradation in the absence of a catalyst is also included for comparison purposes. Initial concentrations in the solution after the preadsorption step: 50 ppm (phenol) and 5 ppm (RhB).

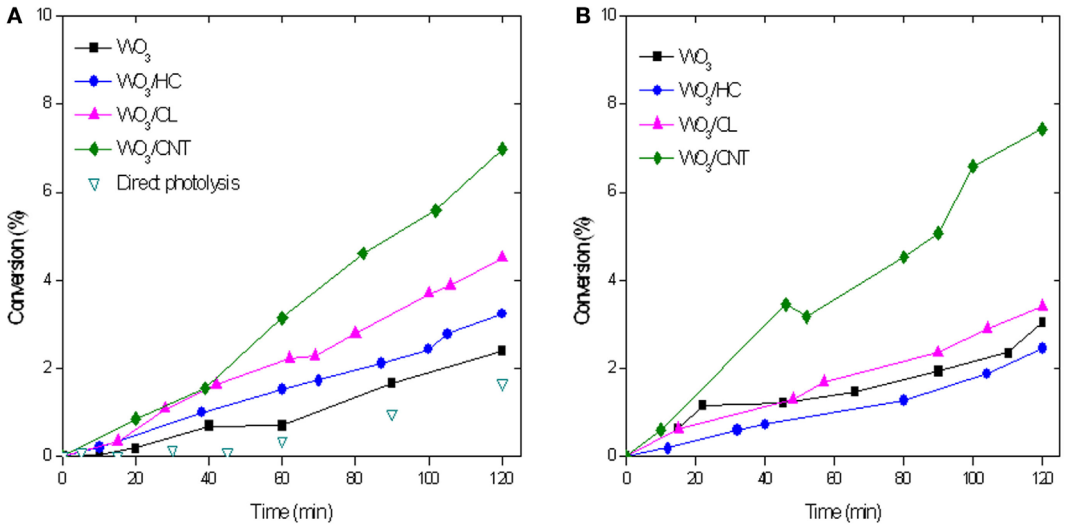

FIGURE 3 | Phenol conversion with a catalyst loading of 0.5 g/L (A) and 1 g/L (B) upon simulated solar light irradiation of the catalysts. 50 mg L^{-1} phenol in solution at the beginning of the illumination.

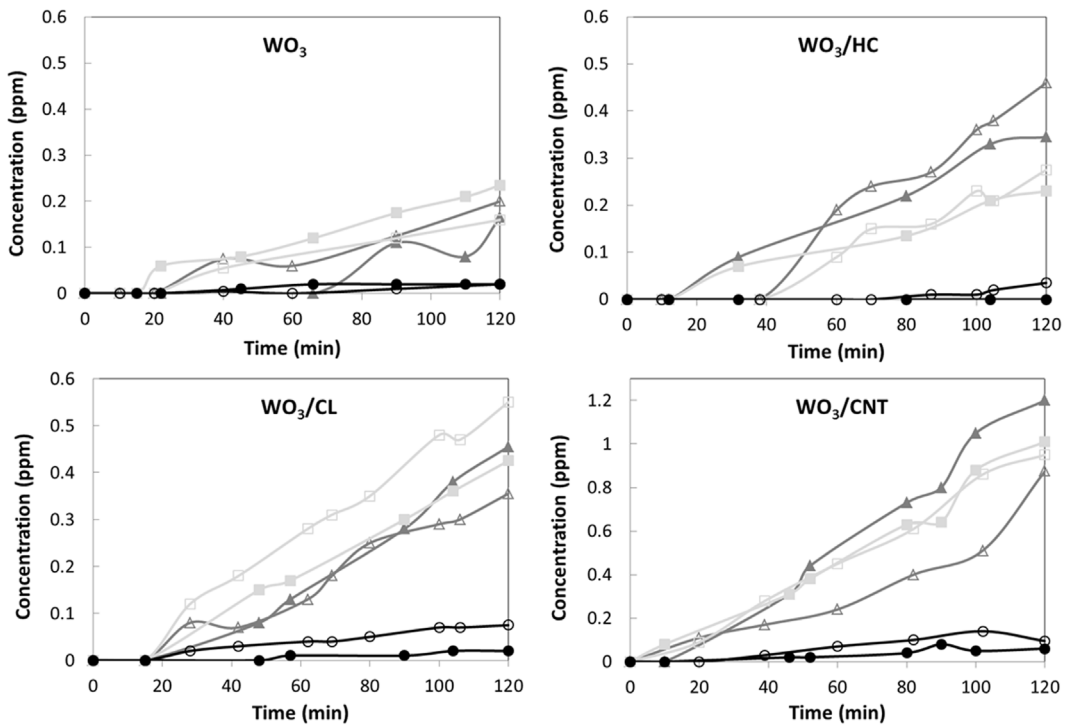

FIGURE 4 | Evolution of the phenol photooxidation intermediates detected in solution upon irradiation of the studied materials for a catalyst loading of 0.5 (open symbols) and 1 g/L (closed symbols): benzoquinone (circles), catechol (triangles), and hydroquinone (squares). 50 mg L^{-1} phenol in solution at the beginning of the illumination.

exception of WO_3/CNT (**Figure 3B**). We attribute this effect to the shielding effect of the catalysts particles dispersed in the solution, that hinder the absorption of light. For WO_3/CNT, both the rate and the yield of the photodegradation process increased with the amount of catalyst, suggesting that the shielding effect of the CNT particles may be counteracted by other effects (likely an improved electron transfer).

Regarding intermediates, dihydroxylated benzenes were the main products detected in solution (**Figure 4**), indicating that the degradation pathway of phenol was similar for all four

studied catalysts. According to literature, phenol is preferentially adsorbed on hydrophobic carbon surfaces via the interaction between the aromatic ring with the adsorbent's surface. Thus, the aromatic ring is easily oxidized via an electrophilic attach of hydroxyl radicals formed upon oxidation of water by the holes, inducing the opening of the aromatic ring to preserve the double bond conjugation (Prakash Reddy and Surya Prakash, 2003). The electrophilic-mediated pathway involving hydroxyl radicals or direct hole oxidation is also confirmed by the predominance of the ortho-dihydroxylated degradation intermediate (catechol). The preferential formation of hydroquinone over benzoquinone was also quite expected, considering the hydrophilic character of all the catalysts (Prakash Reddy and Surya Prakash, 2003; Matos et al., 2010). As for the catalyst loading, it seemed to have a small effect on the photocatalytic efficiency (though more pronounced for WO_3/CNT), other than a slight increase in the amount of intermediates.

It should be reminded that the photocatalytic runs were carried out on the samples initially equilibrated in solution at dark conditions to counteract the different adsorption properties of the catalysts (mainly controlled by the porous features and surface chemistry of the carbon additive). Phenol uptakes corresponding to the photocatalysts were 0.4, 1.9, 2.2, and 2.4 mg phenol/g for WO_3, WO_3/HC, WO_3/CL, and WO_3/CNT, respectively. Also, the contribution of phenol direct photolysis can be neglected (**Table 2**), for which the higher photoactivity exhibited by the WO_3/carbon catalysts as well as the differences in the photodegradation yields cannot be attributed to the removal upon adsorption (only occurring in the preadsorption step) and must be explained by the characteristics of the carbon additives.

Figures 5 and **6** show the correlation of the performance of the hybrid photocatalysts toward the photooxidation of phenol and selected properties of the carbon additives for both catalyst loadings (ca. 0.5 and 1 g/L). As seen, the same trend was obtained

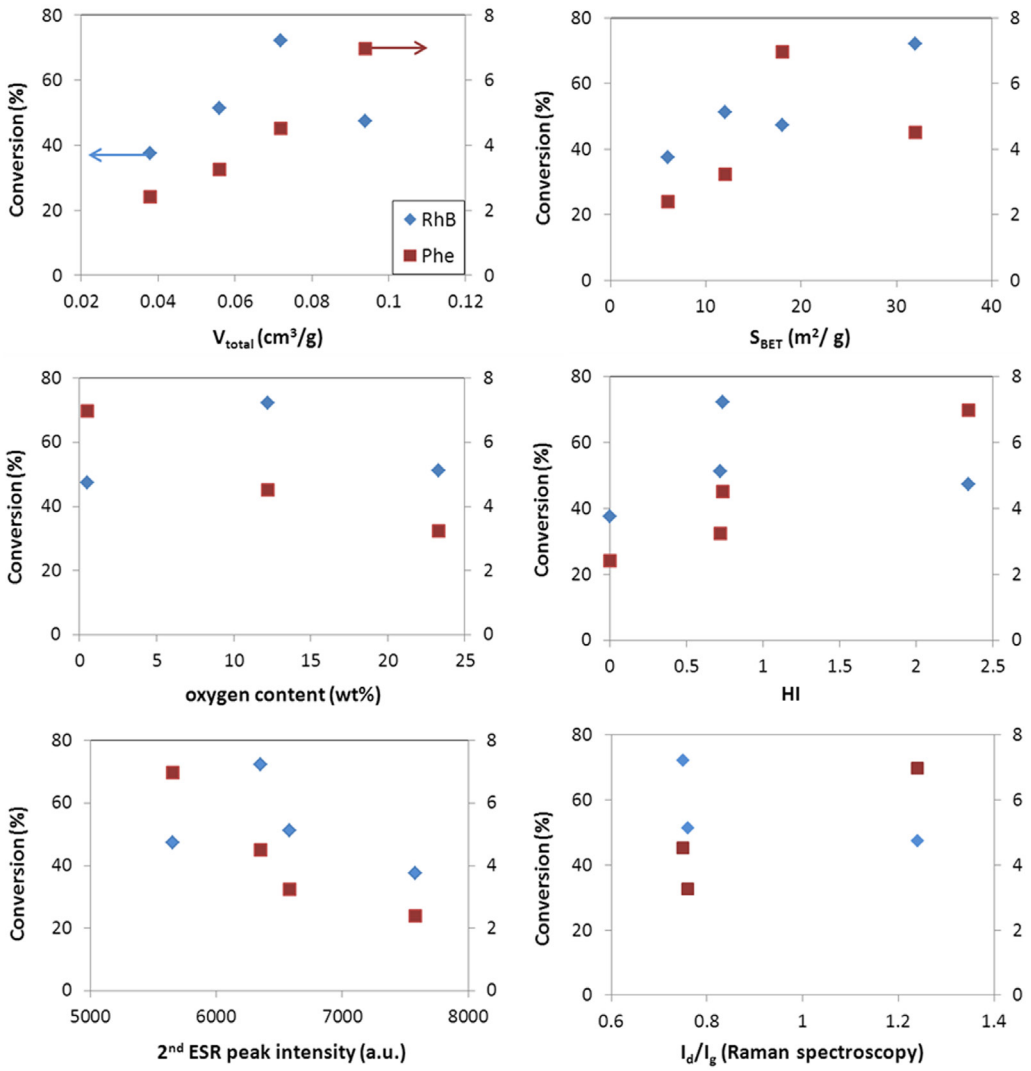

FIGURE 5 | Correlation of conversion values for phenol (right axis) and rhodamine (left axis) with selected characteristics of the WO_3/carbon photocatalysts for a catalyst loading of 0.5 g/L.

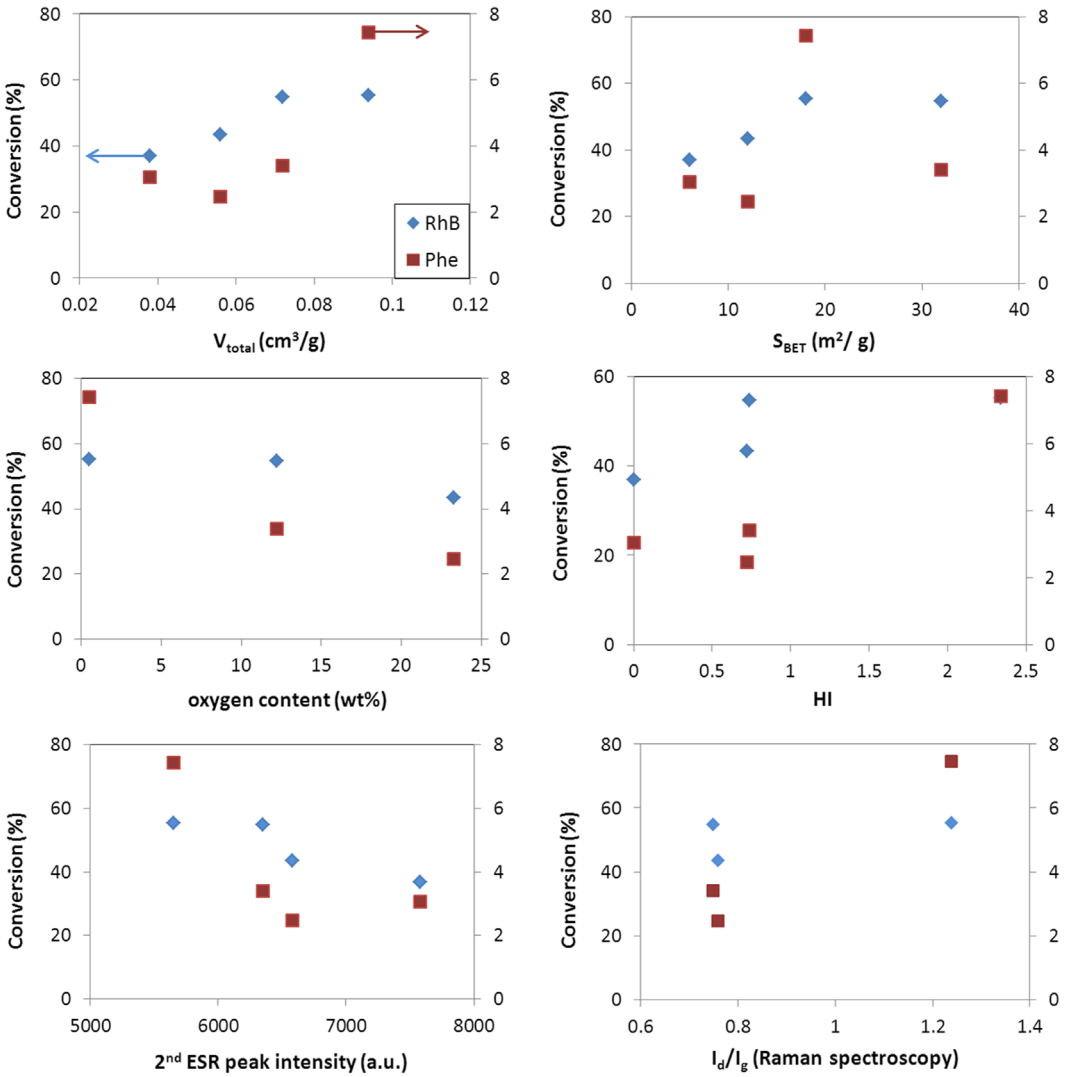

FIGURE 6 | Correlation of conversion values for phenol (right axis) and rhodamine (left axis) with selected characteristics of the WO_3/carbon photocatalysts for a catalyst loading of 1 g/L.

in for both catalyst loadings. A clear correlation is observed with the surface acidity/basicity (in terms of oxygen content and HI). The photodegradation of phenol was superior in the catalysts incorporating basic carbon additives; this shows that the affinity between the catalyst's surface and phenol molecules is critical. In this regard, it is well known that phenol is preferentially adsorbed on hydrophobic (basic) carbon adsorbents (Moreno-Castilla, 2004); hence, a hydrophobic catalyst interface would favor the contact of phenol molecules (in the adsorbed state) close to the photoactive sites of the catalysts, increasing the photooxidation yield. The structural order of the carbon component also seems an important factor, given the superior performance of WO_3/CNT that would be related to the higher structural order and electronic conductivity of the nanotubes (**Figures 5** and **6**). Indeed, it has been reported that carbon nanotubes can act as scavengers of the photogenerated charge carriers favoring their separation and increasing their lifetime due to the large electron mobility (Wang et al., 2005; Faria and Wang, 2009; Woan et al., 2009).

This greater photoactivity exhibited by WO_3/carbon catalysts may be attributed to various reasons: first, the reduction of the electron–hole recombination rate in WO_3 because the electrons can be transferred to the π-electron reservoir of the carbon materials that would be acting as electron sink, alleviating their accumulation on the surface via delocalization in the graphenic layers and hence allowing for greater hole availability for photodegradation reactions. This is expected to be the dominant mechanism applying in the case of WO_3/CNT considering the existence of large graphitic domains in the carbon nanotubes (Figure S2 in Supplementary Material), capable of acting as re effective structure as electron acceptor, in turn enhancing the photocatalytic activity. An effective coupling of WO_3 with the carbon additive is critical to promote the interfacial charge-transfer

phenomena, which in turn extends the lifetime excited charge carriers improving the photocatalytic process. In this case, given the preparation procedure we do not expect to have an optimized contact at the WO_3/carbon interface, for which the occurrence of ordered graphitic domains in the carbon additive become important for an enhanced exploitation of the electron-hole pairs avoiding their recombination.

Second, the porosity of the carbon additives and their hydrophobicity should also be considered. The hydrophobic environment provided by the carbon additive (**Table 2**) favors the adsorption of phenol in the nanopores, as above-mentioned. Dissolved molecular oxygen from the solution is also adsorbed in the pores – the hydrophobic effect of dissolved oxygen in water is due to changes in the clustering of water molecules; the density of water clusters adsorbed in hydrophobic surfaces is low, encouraging non-polar dissolved oxygen gas accumulation (Matsis and Grigoropoulou, 2008; Dastgheib and Karanfil, 2004). The latter, which can boost the participation of the photogenerated electrons in the multielectron reduction of O_2 ($O_2 + 2H^+ + 2e^- = H_2O_2$, and $O_2 + 4H^+ + 2e^- = 2H_2O$), as the π-electron reservoir guarantees the close proximity of more than one electron (needed to favor the multielectron reduction), in a similarly way as reported for metal loaded WO_3 (Ho et al., 2012). The ability of dissolved oxygen to concentrate on the hydrophobic surface of the catalysts at the local environment of the carbon matrix, combined with the enhanced electron transfer properties of the CNT would account for the higher catalytic activity of WO_3/CNT. For WO_3/HC and WO_3/CL, the charge transfer process is limited by the lower conductivity of the carbon phase (**Table 2** and **Figures 5** and **6**), as supported by the HI results and Raman spectroscopy.

Another possibility is the stabilization of the holes through the oxidation of water molecules co-confined in the nanopore space of the carbons, leading to the formation of reactive oxygen species (ROS) necessary for photooxidation reaction. The ability of the hybrid photocatalysts to form radicals was confirmed by spin resonance spectroscopy using a nitrone spin trapping agent (**Figure 7**). Similar ESR patterns were obtained for all the samples, with the characteristic quartet peak profile with 1:2:2:1 intensity (g = 2.006, aN = abH = 14.8 G hyperfine splitting constants) of the DMPO-OH adduct attributed to hydroxyl and superoxide radicals (Finkelstein et al., 1980; Velasco et al., 2013a). Quantification of the relative abundance of ROS showed rather constant concentration levels in the photocatalysts, pointing out that the slightly higher basicity on the surface of WO_3/carbons compared to bare WO_3 does not affect their affinity to generate species with unpaired electrons (i.e., OH radicals). In this regard, it should be noted that the carbon additives used in this work have the capacity themselves to photogenerate ROS upon illumination (Velasco et al., 2013a). Thus, charge carriers are generated as a result of both WO_3–photon and carbon–photon interactions; if splitting is favored (due to existence of reservoir, electron acceptors and hole scavengers), they can propagate and participate in charge transfer reactions (either involving direct hole oxidation due to the proximity of phenol molecules in the adsorbed state, and/or radical mediated mechanisms). All these processes may coexist simultaneously and may contribute to the observed superior activity of the hybrid WO_3/carbon catalysts (Haro et al., 2012; Velasco et al., 2013a).

Rhodamine B Photodegradation

We also investigated the effect of the carbon additive on the photocatalytic degradation of WO_3/carbon catalysts toward RhB, a compound with a different light absorption features compared to phenol (Figure S3 in Supplementary Material). This pollutant absorbs in the visible range (460–600 nm), thus the contribution of direct photolysis upon irradiation of the solution is higher (**Table 2**). Another important observation is that adsorption capacity of RhB of the studied photocatalysts follows a different trend than that above discussed for phenol, as the uptake is largely influenced by the occurrence of specific interactions at the catalyst surface involving the different charged forms of this compound. Indeed, RhB is an amphoteric dye with a permanent positive charge (diethylamino group) and a negative charge upon dissociation of the carboxylic moiety. In our experimental conditions, RhB is in the zwitterionic form in

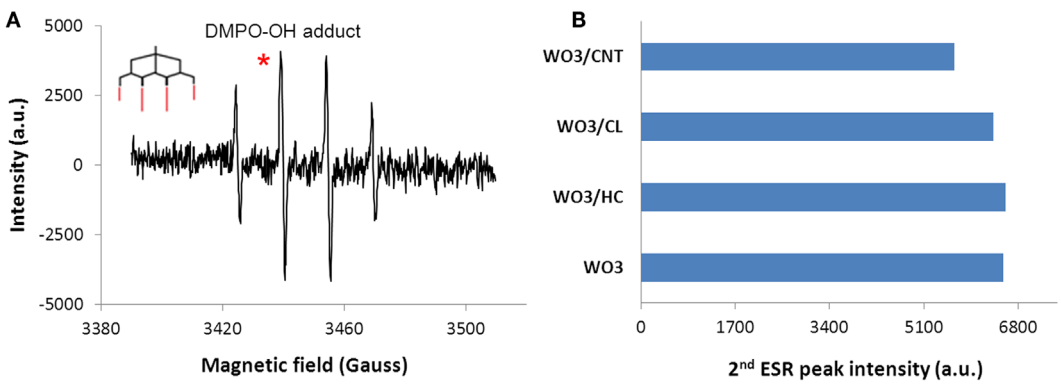

FIGURE 7 | **(A)** Characteristic ESR signal of DMPO-OH adduct (inset) obtained upon 20 min of irradiation of an aqueous suspensions of the WO_3/carbon photocatalysts, **(B)** Quantification of the radical species detected from the ESR signals corresponding to DMPO-OH adducts by integration of the second peak in the 1:2:2:1 quartet profile (marked as*).

the aqueous solution, with predominance of positive charges (Gad and El-Sayed, 2009). Consequently, the uptake is favored in the catalysts of acidic nature (ca. uptakes of 1.2, 1.4, 7.3, and 3.6 mg Rh-B/g for WO_3, WO_3/HC, WO_3/CL, and WO_3/CNT, respectively).

Figure 8 shows the evolution of RhB photoconversion upon 2 h of irradiation of the studied catalysts. As seen, RhB conversions are higher than those obtained for phenol for all the used materials. This is reasonable considering the higher contribution of the photolytic breakdown and the lower initial concentration of RhB used (ca. 5 ppm). It should be clarified that the latter was established considering the typical concentration values of both pollutants in real effluents.

The incorporation of the carbon additive to WO_3 has a marked positive effect on the degradation reaction, with a superior performance of all the hybrid WO_3/carbon catalysts compared to the bare semiconductor (**Table 2** and **Figure 8**). It is noteworthy that the effect of the carbon additive followed a different trend than that observed for the photooxidation of phenol. The photocatalytic performance of WO_3/CL was superior to that obtained with HC and CNT as additives, although both outperformed the bare semiconductor. Similarly to phenol, increasing the catalyst loading to 1 g/L had a small effect on the performance of the photocatalysts, with the exception of WO_3/CL that shows a slightly lower activity (**Table 2** and **Figure 8B**).

As for the characteristics of the carbons, data show a quite clear correlation of the performance with the surface chemistry of the catalysts, being the photodegradation of RhB favored in the catalyst of acidic surface, as opposed to the trend observed for the degradation of phenol. On the contrary, the dependence with the structural order of the carbon additive is not clear, as previously discussed for the conversion of phenol (**Figures 5** and **6**). A similar behavior has been reported for the degradation of RhB using other semiconductors, and attributed to the degradation via coupled mechanisms (photosensitization, photocatalysis, and carbon-photon mediated reactions) in acidic photocatalysts (Galoppini, 2004; Carmona et al., 2015; Wang et al., 2014). Indeed, acidic catalysts' surfaces favor strong interactions with the adsorbed RhB molecules, boosting the degradation via the photosensitization as a result of a more efficient injection of electrons from the dye to the surface of the catalyst. Taking into account the pH of zero charge and HI of the catalysts, the photosensitized mechanism is expected for all of them, especially for WO_3/HC and WO_3/CL (**Table 2** and **Figures 5** and **6**). The better performance of the latter should then be explained also in terms of other properties of the carbon additives. In this regard, CL presents a high developed porosity while HC is a nearly non-porous material (**Table 2**); the porosity of the catalyst provided by CL and CNT is expected to favor the photodegradation reaction through an increased mass transfer of the pollutant from the aqueous media toward the catalyst surface. The beneficial effect of the porosity, in terms of total pore volume and surface area, on the degradation of RhB is more clearly seen in **Figures 5** and **6**. In the case of WO_3/CNT, despite the interactions between RhB and the surface of the catalysts are weaker due to the lower acidity of the carbon additive (**Table 2**), the catalytic performance of the composite still outperforms that of the bare semiconductor (particularly at a catalyst loading of 1 g/L), likely due to the high electron mobility that anticipate a lower recombination of the photogenerated excitons.

Summarizing, all this points out that the effect of the incorporation of carbon additives in the formulation of semiconductors goes beyond the increased surface area and electron mobility reported in the literature and strongly depends on the physicochemical features of the carbon material and the interactions with the target compound.

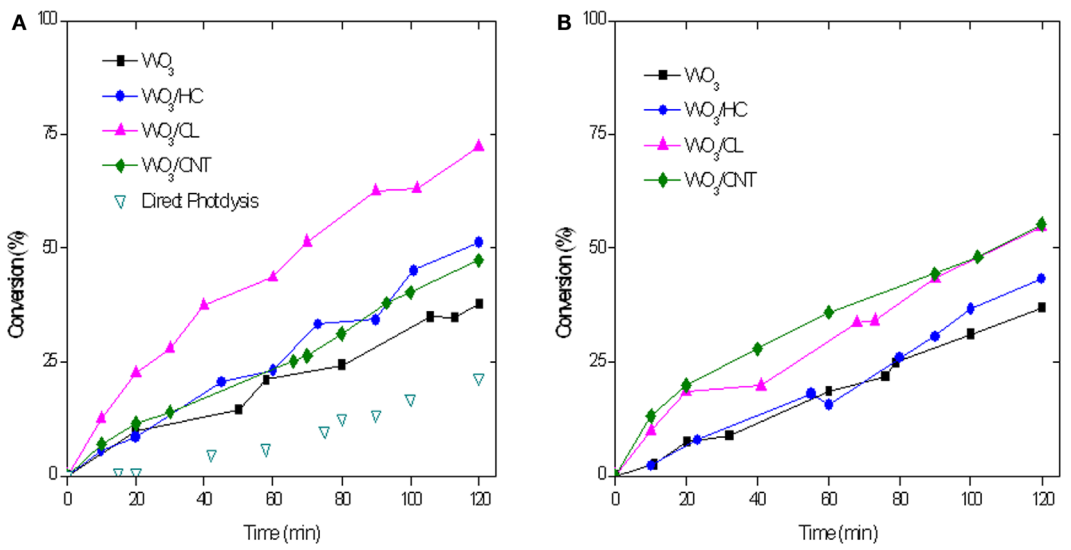

FIGURE 8 | RhB conversion with a catalyst loading of 0.5 g/L (A) and 1 g/L (B) upon simulated solar light irradiation of the catalysts. Five milligram per liter rhodamine B in solution at the beginning of the illumination.

CONCLUSION

We have investigated the role of carbon materials on the photocatalytic performance of WO_3/carbon mixtures toward the degradation of two different pollutants: phenol and Rhodamine-B under simulated solar irradiation. The incorporation of a carbon additive in a low content (ca. 2 wt.%) significantly increased the performance of the semiconductor for the degradation of both pollutants, even though the preparation process of the WO_3/carbon photocatalysts was not optimized the coupling of the carbon component with the semiconductor particles was carried out by simple physical mixture. This is attributed to several factors such as (i) the ability of the carbon additives to act as acceptors contributing to enhance the charge separation through their delocalization in the π-electron density of the graphitic sheets; (ii) the formation of ROS upon irradiation of the photocatalysts; and (iii) the textural and chemical characteristics of the carbon additives. The impact of the carbon additive was different for rhodamine B and phenol, indicating that the performance of a given WO_3/carbon photocatalyst also depends on the nature of the pollutant to be removed. The incorporation of hydrophobic carbon additives to WO_3 increased the photodegradation yield of phenol, which is attributed to the higher affinity and stronger interactions of phenol molecules toward basis nanoporous adsorbents. Alternatively, acidic carbon materials resulted to be more adequate to increase the conversion of RhB from solution; the stronger interactions of RhB adsorbed molecules with the acidic photocatalysts favors a coupled degradation mechanism through the photosensitized process, in addition to the photocatalytic one. All these findings point out that it becomes very crucial to design and tailor the catalyst's properties for a specific application, so as to control the interactions of the target compound with the catalyst's surface, which are governed by the porous and chemical features of both the carbon additive and the semiconductor.

AUTHOR CONTRIBUTIONS

RC is the Ph.D. student who carried out most of the experimental work presented in this paper. CA and LV are the supervisors, who guided her during the present investigation and helped to discuss the results. Both also are the greatest contributors to the writing of the paper and analyze data. VM is the head of the group at the University of Torino where RC carried out a short stay of 3 months and, consequently, he supervised her work during this time. EL is the responsible of the EPR equipment at the University of Torino, who helped to conduct the measurements on the equipment and on data interpretation (included in this paper).

FUNDING

The authors thank the financial support of the Spanish MINECO (grant CTM2014/56770-R). RC thanks PCTI Asturias for her PhD (BP1231, fondos FEDER) fellowship.

SUPPLEMENTARY MATERIAL

The Supplementary Material for this article can be found online at http://journal.frontiersin.org/article/10.3389/fmats.2016.00009

REFERENCES

Ania, C. O., Cabal, B., Parra, J. B., and Pis, J. J. (2007). Importance of hydrophobic character of activated carbons on the removal of naphthalene from aqueous phase. *Adsorpt. Sci. Technol.* 25, 155–168. doi:10.1260/026361707782398164

Ania, C. O., Seredych, M., Rodriguez-Castellon, E., and Bandosz, T. J. (2014). Visible light driven photoelectrochemical water splitting on metal free nanoporous carbon promoted by chromophoric functional groups. *Carbon N. Y.* 79, 432–444. doi:10.1016/j.carbon.2014.08.001

Ania, C. O., Velasco, L. F., and Valdes-Solis, T. (2012). "Photochemical behavior of carbon adsorbents," in *Novel Carbon Adsorbents*, ed. Tascon J. M. D. (Amsterdam: Elsevier), 521–547.

Araña, J., Doña-Rodriguez, J. M., Tello Rendón, E., Garriga i Cabo, C., González-Diaz, C., Herrera Melián, J. A., et al. (2003). TiO_2 activation by using activated carbon as a support. Part II. Photoreactivity and FTIR study. *Appl. Catal.* 44, 153–160.

Bignozzi, C. A., Caramori, S., Cristino, V., Argazzi, R., Meda, L., and Tacca, A. (2013). Nanostructured photoelectrodes based on WO_3: applications to photooxidation of aqueous electrolytes. *Chem. Soc. Rev.* 42, 2228–2246. doi:10.1039/c2cs35373c

Bullett, D. W. (1983). Bulk and surface electron states in WO_3 and tungsten bronzes. *J. Phys. C. Solid State* 16, 2197–2207. doi:10.1088/0022-3719/16/11/022

Carmona, R. J., Velasco, L. F., Hidalgo, M. C., Navío, J. A., and Ania, C. O. (2015). Boosting the visible-light photoactivity of Bi_2WO_6 using acidic carbon additives. *Appl. Cata.* 505, 467–477. doi:10.1016/j.apcata.2015.05.011

Cotton, F. A., and Wilkinson, G. (1988). *Advances in Organic Chemistry*, 5th Edn. New York: Wiley.

Dastgheib, S. A., and Karanfil, T. (2004). Adsorption of oxygen by heat-treated granular and fibrous activated carbons. *J. Colloid Interface Sci.* 274, 1–8. doi:10.1016/j.jcis.2004.01.047

Faria, J. L., and Wang, W. (2009). "Carbon materials in photocatalysis," in *Carbon Materials for Catalysis*, eds Serp P. and Figueiredo J. L. (New York: John Wiley & Sons), 481–506.

Finkelstein, E., Rosen, G. M., and Rauckman, E. (1980). Spin trapping of superoxide and hydroxyl radical: practical aspects. *J. Arch. Biochem. Biophys.* 200, 1–16. doi:10.1016/0003-9861(80)90323-9

Gad, H., and El-Sayed, A. A. (2009). Activated carbon from agricultural by-products for the removal of Rhodamine-B from aqueous solution. *J. Hazard. Mater.* 168, 1070–1081. doi:10.1016/j.jhazmat.2009.02.155

Galoppini, E. (2004). Linkers for anchoring sensitizers to semiconductor nanoparticles. *Coord. Chem. Rev.* 248, 1283–1297. doi:10.1016/j.ccr.2004.03.016

Gratzel, M. (2001). Photolectrochemical cells. *Nature* 414, 338–344. doi:10.1038/35104607

Haro, M., Velasco, L. F., and Ania, C. O. (2012). Carbon-mediated photoinduced reactions as a key factor in the photocatalytic performance of C/TiO_2. *Catal. Sci. Technol.* 2, 2264–2272. doi:10.1039/c2cy20270k

Hjelm, A., Granqvist, C. G., and Wills, J. M. (1996). Electronic structure and optical properties of WO_3, $LiWO_3$, $NaWO_3$, and HWO_3. *Phys. Rev.* 54, 2436–2445. doi:10.1103/PhysRevB.54.2436

Ho, G. W., Chua, K. J., and Siow, D. R. (2012). Metal loaded WO_3 particles for comparative studies of photocatalysis and electrolysis solar hydrogen production. *Chem. Eng. J.* 18, 661–666. doi:10.1016/j.cej.2011.12.039

Irie, H., Miura, S., Kamiya, K., and Hashimoto, K. (2008). Efficient visible light-sensitive photocatalysts: grafting Cu(II) ions onto TiO_2 and WO_3 photocatalysts. *Chem. Phys. Lett.* 457, 202–205. doi:10.1016/j.cplett.2008.04.006

Kopp, L., Harmon, B. N., and Liu, S. H. (1977). Band structure of cubic Na_xWO_3. *Solid State Commun.* 22, 677–679. doi:10.1016/0038-1098(77)90248-4

Kubelka, P. (1948). New contributions to the optics of intensely light-scattering materials. *J. Opt. Soc. Am.* 38, 448–457. doi:10.1364/JOSA.38.001067

Kuhn, H. K., Braslavsky, S. E., and Schmidt, R. (2004). Chemical actinometry (IUPAC technical report). *Pure Appl. Chem.* 76, 2105–2146. doi:10.1351/pac200476122105

Kumar, S. G., and Rao, K. S. R. K. (2015). Tungsten-based nanomaterials (WO_3 & Bi_2WO_6): modifications related to charge carrier transfer mechanisms and photocatalytic applications. *Appl. Surf. Sci.* 355, 939–958. doi:10.1016/j.apsusc.2015.07.003

Leary, R., and Westwood, A. (2011). Carbonaceous nanomaterials for the enhancement of TiO_2 photocatalysis. *Carbon N. Y.* 49, 741–742. doi:10.1016/j.carbon.2010.10.010

Matos, J., García, A., and Poon, P. S. (2010). Environmental green chemistry applications of nanoporous carbons. *J. Mater. Sci.* 45, 4934–4944. doi:10.1007/s10853-009-4184-2

Matsis, V. M., and Grigoropoulou, H. P. (2008). Kinetics and equilibrium of dissolved oxygen adsorption on activated carbon. *Chem. Eng. Sci.* 63, 609–621. doi:10.1016/j.ces.2007.10.005

Moreno-Castilla, C. (2004). Adsorption of organic molecules from aqueous solutions on carbon materials. *Carbon N. Y.* 42, 83–94. doi:10.1016/j.carbon.2003.09.022

Nosaka, Y., Takahashi, S., Sakamoto, H., and Nosaka, A. Y. (2011). Reaction mechanism of Cu(II)-grafted visible-light responsive TiO_2 and WO_3 photocatalysts studied by means of ESR spectroscopy and chemiluminescence photometry. *J. Phys. Chem. C* 115, 21283–21290. doi:10.1021/jp2070634

Prakash Reddy, V., and Surya Prakash, G. K. (2003). "Electrophilic reactions of phenols," in *The Chemistry of Phenols*, ed. Rappoport Z. (England: John Wiley & Sons), 600–660.

Rouquerol, F., Rouquerol, J., Sing, K. S. W., Llewellyn, P., and Maurin, G. (2014). *Adsorption by Powders and Porous Solids: Principles, Methodology and Applications*, 2nd Edn. Oxford: Elsevier.

Spurgeon, J. M., Velazquez, J. M., and McDowell, M. T. (2014). Improving O_2 production of WO_3 photoanodes with IrO_2 in acidic aqueous electrolyte. *Phys. Chem. Chem. Phys.* 16, 3623–3631. doi:10.1039/c3cp55527e

Svensson, J. S. E. M., and Granqvist, C. G. (1984). Electrochromic tungsten oxide films for energy efficient windows. *Sol. Energy Mater.* 11, 29–34. doi:10.1016/0165-1633(84)90025-X

Velasco, L. F., Fonseca, I. M., Parra, J. B., Lima, J. C., and Ania, C. O. (2012). Photochemical behaviour of activated carbons under UV irradiation. *Carbon N. Y.* 50, 249–258. doi:10.1016/j.carbon.2011.08.042

Velasco, L. F., Lima, J. C., and Ania, C. O. (2014). Visible-light photochemical activity of nanoporous carbons under monochromatic light. *Angew. Chem. Int. Ed.* 53, 4146–4148. doi:10.1002/anie.201400887

Velasco, L. F., Maurino, V., Laurenti, E., and Ania, C. O. (2013a). Light-induced generation of radicals on semiconductor-free carbon photocatalysts. *Appl. Catal.* 453, 310–315. doi:10.1016/j.apcata.2012.12.033

Velasco, L. F., Haro, M., Parmentier, J., Gadiou, R., Vix-Guterl, C., and Ania, C. O. (2013b). Tuning the photocatalytic activity and optical properties of mesoporous TiO_2 spheres by a carbon scaffold. *J. Catal.* 2013, 9. doi:10.1155/2013/178512

Wang, P., Cheng, M., and Zhang, Z. (2014). On different photodecomposition behaviors of rhodamine B on laponite and montmorillonite clay under visible light irradiation. *J. Saudi. Chem. Soc.* 18, 308–316.

Wang, W. D., Serp, P., Kalck, P., and Faria, J. L. (2005). Visible light photodegradation of phenol on MWNT-TiO2 composite catalysts prepared by a modified sol–gel method. *J. Mol. Catal.* 235, 194–199. doi:10.1016/j.molcata.2005.02.027

Wen, Z., Wu, W., Liu, Z., Zhang, H., Li, J., and Chen, J. (2013). Ultrahigh-efficiency photocatalysts based on mesoporous Pt–WO_3 nanohybrids. *Phys. Chem. Chem. Phys.* 15, 6773–6778.

Wicaksana, Y., Liu, S., Scott, J., and Amal, R. (2014). Tungsten trioxide as a visible light photocatalyst for volatile organic carbon removal. *Molecules* 19, 17747–17762. doi:10.3390/molecules191117747

Woan, K., Pyrgiotakis, G., and Sigmund, W. (2009). Photocatalytic carbon-nanotube–TiO_2 composites. *Adv. Mater.* 21, 2233–2239. doi:10.1002/adma.200802738

Conflict of Interest Statement: The authors declare that the research was conducted in the absence of any commercial or financial relationships that could be construed as a potential conflict of interest.